

Multi-orbital analysis on the Superconductivity in $\text{Na}_x\text{CoO}_2 \cdot y\text{H}_2\text{O}$

Youichi YANASE,* Masahito MOCHIZUKI and Masao OGATA

Department of Physics, University of Tokyo, Tokyo 113-0033

(Received Today 2004)

We perform a multi-orbital analysis on the novel superconductivity in $\text{Na}_x\text{CoO}_2 \cdot y\text{H}_2\text{O}$. We construct a three-orbital model which reproduces the band structure expected from the LDA calculation. The effective interaction leading to the pairing is estimated by means of the perturbation theory. It is shown that the spin triplet superconductivity is stabilized in the wide parameter region. This is basically owing to the ferromagnetic character of spin fluctuation. The *p*-wave and *f*-wave superconductivity are nearly degenerate. The former is realized when the Hund's rule coupling is large, and vice versa. In a small part of the parameter space, the *d*-wave superconductivity is also stabilized. We point out that the orbital degeneracy plays an essential role for these results through the wave function of quasi-particles. The nearly degeneracy of *p*-wave and *f*-wave superconductivity is explained by analysing the orbital character of each Fermi surface. We discuss the validity of some reduced models. While the single band Hubbard model reproducing the Fermi surface is qualitatively inappropriate, we find an effective two-orbital model appropriate for studying the superconductivity. We investigate the vertex corrections higher than the third order on the basis of the two-orbital model. It is shown that the vertex correction induces the screening effect but does not affect on the qualitative results.

KEYWORDS: $\text{Na}_x\text{CoO}_2 \cdot y\text{H}_2\text{O}$; unconventional superconductivity; ferromagnetic spin fluctuation; multi-orbital analysis

1. Introduction

Since the discovery of High- T_c superconductivity¹⁾ and heavy fermion superconductors,²⁾ the mechanism of superconductivity induced by electron correlation has been one of the central issues in the condensed matter physics. In this study, recently discovered superconductor $\text{Na}_x\text{CoO}_2 \cdot y\text{H}_2\text{O}$ is analyzed in details.

Immediately after the discovery of superconductivity in water-intercalated Cobalt oxides $\text{Na}_x\text{CoO}_2 \cdot y\text{H}_2\text{O}$,³⁾ both experimental^{4–18)} and theoretical^{19–30)} studies have been performed extensively. While some controversial results exist, many experimental evidences for the non-*s*-wave superconductivity has been reported by NMR^{10–13)} and specific heat measurements.^{17, 18)} The characteristic behaviors in strongly correlated electron systems have been observed in the non-water-intercalated compounds.^{7–9, 31)} The existence of the magnetic phase^{4–6)} in Na_xCoO_2 with $x \sim 0.75$ also indicates an importance of electron correlation. These compounds have a layered structure like cuprate¹⁾ and ruthenate,³²⁾ and the two-dimensionality is enhanced by the water-intercalation. These circumstantial evidences indicate that $\text{Na}_x\text{CoO}_2 \cdot y\text{H}_2\text{O}$ is an unconventional superconductor induced by the electron correlation.

The theoretical interests are turned on also by the symmetry of crystal structure. In contrast to the square lattice in cuprates and ruthenates, the layer is constructed from the triangular lattice of Co ions. Then, a novel symmetry of Cooper pairing is possible in principle. The *d*-wave superconductivity in cuprate superconductors and *p*-wave superconductivity in ruthenates have been established before. In addition to them, the spin triplet *f*-wave superconductivity and spin singlet *i*-wave one are possi-

ble from the analysis of pairing symmetry (see Table. I).

The effect of frustration which is characteristic in the spin system on triangular lattice has also attracted much attention. The RVB theory has been applied to the triangular lattice^{21–24)} and basically concluded the spin singlet *d*-wave superconductivity. Then, $d_{x^2-y^2} \pm id_{xy}$ -wave symmetry is expected below T_c owing to the six-fold symmetry of triangular lattice. However, the time-reversal symmetry breaking has not been observed until now.¹⁴⁾ Some authors have pointed out the frustration of charge ordering for the electron filling $n = 4/3$,²³⁾ and the *f*-wave superconductivity due to the charge fluctuation has been discussed.^{27, 30)}

Another interesting property of $\text{Na}_x\text{CoO}_2 \cdot y\text{H}_2\text{O}$ is the orbital degeneracy. The conduction band of this material mainly consists of three t_{2g} -orbitals in Co ions which hybridize with O2p-orbitals. Thus far, most of theoretical studies on the superconductivity have been performed on the basis of the single-orbital model. These investigations have successfully achieved microscopic understandings on the cuprate, organic and ruthenate superconductors.³³⁾ However, we consider that the theoretical analysis including the orbital degeneracy is highly desired in order to understand a variety of superconductors including the heavy fermion compounds. The superconductivity in *d*-electron systems provides a favorable subject for the theoretical development along this line, because a simple electronic structure is expected compared to heavy fermion superconductors. Although Sr_2RuO_4 has been a precious compound in this sense, then the orbital degree of freedom is not important for the basic mechanism of superconductivity.^{34, 35)} In this study, we show that the orbital degeneracy plays an essential role in $\text{Na}_x\text{CoO}_2 \cdot y\text{H}_2\text{O}$ in contrast to ruthenate superconductor.

*yanase@hosi.phys.s.u-tokyo.ac.jp

We adopt the perturbative method for the unconventional superconductivity,³³⁾ which is a systematic approach for the electron correlation. Note that the spin fluctuation theory³⁶⁾ which is widely used for superconductivity is microscopically formulated in this method. It is expected that this approach is reliable from weak to intermediate coupling region. Before the discovery of $\text{Na}_x\text{CoO}_2 \cdot y\text{H}_2\text{O}$, this method has been applied to the single-orbital triangular lattice. Then, the *d*-wave,³⁷⁾ *f*-wave³⁸⁾ and *p*-wave superconductivity³⁹⁾ have been observed for various electron fillings. Some authors have applied this calculation to $\text{Na}_x\text{CoO}_2 \cdot y\text{H}_2\text{O}$, and reported the spin singlet *d*- or *i*-wave superconductivity,²⁵⁾ spin triplet *f*-wave superconductivity²⁸⁾ and nearly degeneracy between *d*- and *f*-wave superconductivity.²⁹⁾ We consider that this puzzling problem should be resolved by the multi-orbital analysis involving the microscopic aspects of electronic structure.

In this paper, we analyze a multi-orbital Hubbard model constructed from three Co t_{2g} -orbitals. This model appropriately reproduces the electronic structure obtained in the LDA calculation.^{40, 41)} The wave function of quasi-particles, which is neglected in the single-orbital Hubbard models, is appropriately taken into account in this multi-orbital model. We show that the momentum dependence of this wave function plays an essential role for the mechanism of superconductivity. We determine the most stable superconducting state with use of the perturbation theory. According to the results of second order perturbation (SOP), third order perturbation (TOP) and renormalized third order perturbation (RTOP) theories, it is concluded that the spin triplet *p*-wave or *f*-wave superconductivity is stable in the wide region of parameter space. The pairing interaction is closely related to the ferromagnetic character of spin susceptibility, although the pairing interaction is not simply described by the spin susceptibility like in the single band model.³³⁾ While the momentum dependence of spin susceptibility is usually not remarkable in the frustrating system, the ferromagnetic character clearly appears in the present case owing to the orbital degree of freedom.

From a comparison with single-orbital Hubbard models, the important roles of orbital degeneracy are illuminated in §4.1. Alternatively, we propose a reduced two-orbital model including the e_g -doublet (§4.2). It is shown that results for the superconductivity is appropriately reproduced in this simplified model. On the basis of the two-orbital model, we investigate the roles of vertex correction terms (§5). Then, we show that the vertex correction term, which significantly enhances the spin triplet pairing in Sr_2RuO_4 ,³⁴⁾ is not important in case of $\text{Na}_x\text{CoO}_2 \cdot y\text{H}_2\text{O}$. Thus, the superconducting instability is basically described within the SOP. Therefore, we first explain in details the results of SOP in §3, and discuss the reduced models in §4 and the role of vertex corrections in §5.

2. Multi-orbital model

First, we construct a multi-orbital model for $\text{Na}_x\text{CoO}_2 \cdot y\text{H}_2\text{O}$.⁴²⁾ We consider a two-dimensional model which represents the Co ions on the trian-

gular lattice. Note that the superconductivity occurs when the two-dimensionality is enhanced by the water-intercalation. We also note that the conduction band mainly consists of Co t_{2g} -orbitals.^{40, 41)} Co ion is enclosed by an octahedron of oxygens and nearest neighbor Co ions share the edge of the octahedron. We describe the dispersion relation by using a tight-binding model and adopt a multi-orbital Hubbard Hamiltonian written as,

$$H_3 = H_0 + H_1, \quad (1)$$

$$H_0 = \sum_{i,j,s} \sum_{a,b} t_{a,b,i,j} c_{i,a,s}^\dagger c_{j,b,s}, \quad (2)$$

$$\begin{aligned} H_1 = & U \sum_i \sum_a n_{i,a,\uparrow} n_{i,a,\downarrow} + U' \sum_i \sum_{a>b} n_{i,a} n_{i,b} \\ & - J_H \sum_i \sum_{a>b} (2S_{i,a} S_{i,b} + \frac{1}{2} n_{i,a} n_{i,b}) \\ & + J \sum_i \sum_{a \neq b} c_{i,a,\downarrow}^\dagger c_{i,a,\uparrow}^\dagger c_{i,b,\uparrow} c_{i,b,\downarrow}. \end{aligned} \quad (3)$$

The first term H_0 is a tight-binding Hamiltonian where $t_{a,b,i,j}$ are hopping matrix elements. Here, the indices i and j denote the cites in the real space and indices a and b denote the orbitals. We assign the d_{xy} -, d_{yz} - and d_{xz} -orbitals to $a = 1$, $a = 2$ and $a = 3$, respectively. The largest matrix element is the inter-orbital hopping through O2p-orbitals, which are $t_{1,2,i,j}$ for $j = i \pm (\mathbf{a} + \mathbf{b})$, $t_{2,3,i,j}$ for $j = i \pm \mathbf{a}$ and $t_{1,3,i,j}$ for $j = i \pm \mathbf{b}$. We choose the lattice constant as a unit length and denote the unit vectors as $\mathbf{a} = (\sqrt{3}/2, -1/2)$ and $\mathbf{b} = (0, 1)$ which are the basis of the triangular lattice. If we assume only the largest matrix elements, the system is regarded to be a superposition of the kagome lattice.²⁰⁾ However, the long range hopping through the O2p-orbitals and direct hopping between Co ions are needed to reproduce the Fermi surface obtained in the LDA calculation.

We take account of the matrix elements within third-nearest-neighbor cites according to the symmetry of orbitals and lattice. They are described by nine parameters from t_1 to t_9 . The non-interacting Hamiltonian is described in the matrix representation,

$$H_0 = \sum_{\mathbf{k},s} c_{\mathbf{k},s}^\dagger \hat{H}(\mathbf{k}) c_{\mathbf{k},s}, \quad (4)$$

$$\hat{H}(\mathbf{k}) = \begin{pmatrix} \varepsilon_{11}(\mathbf{k}) & \varepsilon_{12}(\mathbf{k}) & \varepsilon_{13}(\mathbf{k}) \\ \varepsilon_{21}(\mathbf{k}) & \varepsilon_{22}(\mathbf{k}) & \varepsilon_{23}(\mathbf{k}) \\ \varepsilon_{31}(\mathbf{k}) & \varepsilon_{32}(\mathbf{k}) & \varepsilon_{33}(\mathbf{k}) \end{pmatrix}, \quad (5)$$

where $c_{\mathbf{k},s}^\dagger = (c_{\mathbf{k},1,s}^\dagger, c_{\mathbf{k},2,s}^\dagger, c_{\mathbf{k},3,s}^\dagger)$ is a vector representation of the Fourier transformed creation operators with spin s . The matrix elements are obtained as,

$$\begin{aligned} \varepsilon_{11}(\mathbf{k}) = & 2t_1 \cos k_1 + 2t_2 (\cos k_2 + \cos k_3) \\ & + 2t_4 (\cos(k_1 - k_3) + \cos(k_1 - k_2)) + 2t_5 \cos 2k_1, \end{aligned} \quad (6)$$

$$\begin{aligned} \varepsilon_{22}(\mathbf{k}) = & 2t_1 \cos k_2 + 2t_2 (\cos k_1 + \cos k_3) \\ & + 2t_4 (\cos(k_1 - k_2) + \cos(k_2 - k_3)) + 2t_5 \cos 2k_2, \end{aligned} \quad (7)$$

$$\begin{aligned} \varepsilon_{33}(\mathbf{k}) = & 2t_1 \cos k_3 + 2t_2 (\cos k_1 + \cos k_2) \\ & + 2t_4 (\cos(k_1 - k_3) + \cos(k_2 - k_3)) + 2t_5 \cos 2k_3, \end{aligned} \quad (8)$$

$$\begin{aligned}\varepsilon_{12}(\mathbf{k}) &= 2t_3 \cos k_3 + 2t_6 \cos 2k_3 + 2t_7 \cos(k_1 - k_3) \\ &+ 2t_8 \cos(k_2 - k_3) + t_9 \cos(k_1 - k_2) - e_c/3, \quad (9)\end{aligned}$$

$$\begin{aligned}\varepsilon_{13}(\mathbf{k}) &= 2t_3 \cos k_2 + 2t_6 \cos 2k_2 + 2t_7 \cos(k_2 - k_3) \\ &+ 2t_8 \cos(k_1 - k_2) + t_9 \cos(k_1 - k_3) - e_c/3, \quad (10)\end{aligned}$$

$$\begin{aligned}\varepsilon_{23}(\mathbf{k}) &= 2t_3 \cos k_1 + 2t_6 \cos 2k_1 + 2t_7 \cos(k_1 - k_2) \\ &+ 2t_8 \cos(k_1 - k_3) + t_9 \cos(k_2 - k_3) - e_c/3, \quad (11)\end{aligned}$$

where $k_1 = \sqrt{3}/2k_x - 1/2k_y$, $k_2 = k_y$ and $k_3 = -k_1 - k_2$. The parameter e_c represents the crystal field splitting of t_{2g} -orbitals arising from the distortion of octahedron. A typical dispersion relation and Fermi surface are shown in Fig. 1. There is a hole pocket enclosing the Γ -point and six hole pockets near the K -points, which are consistent with LDA calculations.^{40, 41)} We choose the unit of energy as $t_3 = 1$ throughout this paper.

Although e_c seems to be small, it is useful to use a non-degenerate a_{1g} -orbital and doubly-degenerate e_g -orbitals. They are defined from the three t_{2g} -orbitals as

$$|e_g, 1\rangle = \frac{1}{\sqrt{2}}(|xz\rangle - |yz\rangle), \quad (12)$$

$$|e_g, 2\rangle = \frac{1}{\sqrt{6}}(2|xy\rangle - |xz\rangle - |yz\rangle), \quad (13)$$

$$|a_{1g}\rangle = \frac{1}{\sqrt{3}}(|xy\rangle + |xz\rangle + |yz\rangle). \quad (14)$$

The wave function of a_{1g} -orbital spreads along the c -axis, and those of e_g -orbitals spread along the two-dimensional plane. We will show later that this representation is appropriate for understanding the mechanism of superconductivity (§4.2).

The hole pocket around the Γ -point in Fig. 1(a) mainly consists of the a_{1g} -orbital and the six hole pockets near the K -points mainly consists of the e_g -orbitals. Thus, we denote these Fermi surfaces as a_{1g} -Fermi surface and e_g -Fermi surface, respectively. This nature of the Fermi surface is consistent with the LDA calculation.^{40, 41)} Note that recent ARPES measurements^{43, 44)} for non-superconducting Na_xCoO_2 observed the a_{1g} -Fermi surface, but the e_g -Fermi surface has not been found. Fermi surface of water-intercalated Na_xCoO_2 is not clear at present. Moreover, the valence of Co ion in superconducting materials is also under debate.⁴⁵⁾ Therefore, we investigate a wide region in the parameter space to study the possible pairing instability. It will be shown that the superconductivity is hard to be stabilized when e_g -Fermi surface vanishes.

The second term H_1 describes the short range Coulomb interactions which include the intra-orbital repulsion U , inter-orbital repulsion U' , Hund's rule coupling J_H and pair hopping term J . The relations $U = U' + J_H + J$ and $J_H = J$ are satisfied in a simple estimation. Under these conditions, the interaction term H_1 is invariant for the local unitary transformation between orbitals which will be used later. If these relations are violated, the symmetry of triangular lattice is artificially broken. Therefore, we impose these relations through this paper. Although possible roles of the long range Coulomb interaction have been investigated,^{21, 27, 30)} we concentrate on the short

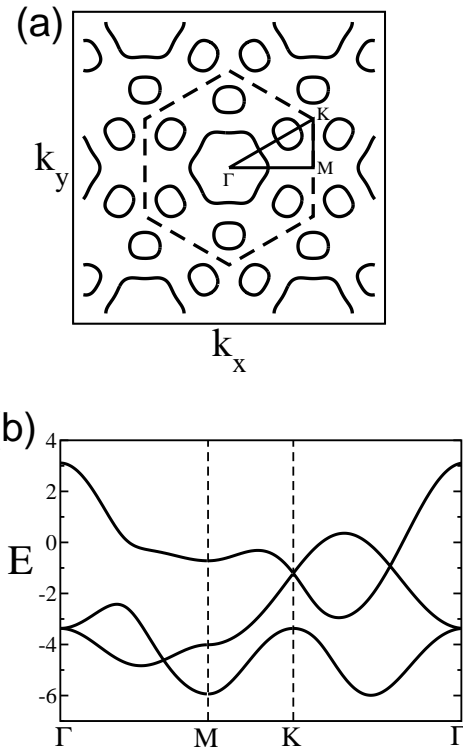


Fig. 1. (a) Fermi surfaces and (b) dispersion relation obtained from the tight-binding Hamiltonian. The dashed line in (a) shows the first Brillouin zone. The parameters are chosen to be $(t_1, t_2, t_3, t_4, t_4, t_5, t_6, t_7, t_8, t_9) = (0.08, 0.16, 1, 0.24, -0.16, -0.04, 0.16, 0.16, -0.2)$.

range interaction in this paper.

Note that previous studies based on a perturbative method for cuprates, organics and ruthenate have succeeded in identifying the dominant scattering process leading to the superconductivity.³³⁾ In this study we apply a perturbation theory to the multi-orbital Hubbard model, which is expected to be reliable from weak to intermediate coupling region. This theory is complementary to the fluctuation theory which is represented by a random phase approximation (RPA) or fluctuation exchange approximation (FLEX). Generally speaking, the fluctuation theory will be appropriate in the vicinity of the magnetic or other instabilities, because the critical enhancement of the fluctuation is taken into account. On the other hand, the perturbation theory is more appropriate when the critical enhancement of a particular fluctuation is absent, because all terms in the same order are taken into account without any prejudice. We perform the second order perturbation as well as the third order perturbation in this paper. The results of FLEX study will be published elsewhere.⁴²⁾

3. Second Order Perturbation

3.1 Details of calculation and classification of pairing symmetry

In this section, we investigate the superconducting instability by using the Éliashberg equation within the second order perturbation (SOP). The basic procedure has been explained in literatures and the extension to

multi-orbital model is straightforward. The Éliashberg equation is described by the Green function and the effective interaction. The latter is represented by an irreducible four point vertex in the particle-particle channel (Fig. 2(a)). The second order terms in the effective interaction are diagrammatically represented by Figs. 2(b-e). In case of the single band Hubbard model, this term is simply expressed as $V(k, k') = U^2 \chi_0(k - k')$ for spin singlet pairing and $V(k, k') = -U^2 \chi_0(k - k')$ for spin triplet pairing, respectively, with a bare spin susceptibility $\chi_0(k - k')$. However, in the multi-orbital model, the four point vertex has indices of orbitals as $V_{abcd}(k, k')$ (see Fig. 2(a)), which is calculated from the possible combination of Coulomb interactions and Green functions.

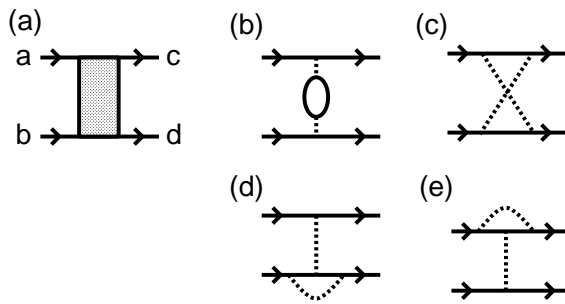


Fig. 2. (a) Diagrammatic representation of the effective interaction leading to the superconductivity. (b-e) The second order terms with respect to the Coulomb interactions (dashed lines). The solid line denotes the Green function having the indices of spin and orbital.

In order to make the following discussions clear, we introduce a unitary transformation $\hat{U}(\mathbf{k}) = (u_{ij}(\mathbf{k}))$ which diagonalizes $\hat{H}(\mathbf{k})$, namely

$$\hat{U}^\dagger(\mathbf{k}) \hat{H}(\mathbf{k}) \hat{U}(\mathbf{k}) = \begin{pmatrix} E_1(\mathbf{k}) & 0 & 0 \\ 0 & E_2(\mathbf{k}) & 0 \\ 0 & 0 & E_3(\mathbf{k}) \end{pmatrix}. \quad (15)$$

Here, we choose $E_1(\mathbf{k}) \leq E_2(\mathbf{k}) \leq E_3(\mathbf{k})$. With use of these matrix elements, the matrix form of Green function characterized by orbitals $\hat{G}(\mathbf{k}) = (i\omega_n \hat{1} - \hat{H}(\mathbf{k}))^{-1}$ is described as,

$$G_{ij}(k) = \sum_{\alpha=1}^3 u_{i\alpha}(\mathbf{k}) u_{j\alpha}(\mathbf{k}) G_\alpha(k), \quad (16)$$

where $G_\alpha(k) = \frac{1}{i\omega_n - E_\alpha(\mathbf{k})}$.

In the following, we denote the energy band described by the dispersion relation $E_3(\mathbf{k})$ as γ -band. As we have shown in Fig. 1, the γ -band crosses the Fermi level, and the others are below the Fermi level. Therefore, the superconducting transition is induced by the Cooper pairing in the γ -band. In this case, the Éliashberg equation is written in terms of an effective interaction within the γ -band,

$$\lambda_e \Delta(k) = - \sum_{k'} V(k, k') |G_3(k')|^2 \Delta(k'), \quad (17)$$

with

$$V(k, k') = \sum_{abcd} u_{a3}(\mathbf{k}) u_{b3}(-\mathbf{k}) V_{abcd}(k, k') u_{c3}(\mathbf{k}') u_{d3}(-\mathbf{k}'). \quad (18)$$

The Éliashberg equation (eq. (17)) is regarded to be an eigenvalue equation and λ_e represents the maximum eigenvalue. The superconducting transition temperature is determined by the criterion $\lambda_e = 1$. Here, we have ignored the normal self-energy which represents de-pairing effects. Although this contribution is important for a quantitative estimation of T_c , qualitative nature of the superconductivity, such as the pairing symmetry and the pairing mechanism, is not usually affected.³³⁾

A ₁	<i>s</i> -wave	1
E ₂	<i>d</i> -wave	$\sin \frac{\sqrt{3}}{2} k_x \sin \frac{1}{2} k_y$
A ₂	<i>i</i> -wave	$\sin \frac{3\sqrt{3}}{2} k_x \sin \frac{1}{2} k_y + \sin \frac{\sqrt{3}}{2} k_x \sin \frac{5}{2} k_y - \sin \sqrt{3} k_x \sin 2 k_y$
E ₁	<i>p</i> -wave	$\sin \frac{1}{2} k_y \cos \frac{\sqrt{3}}{2} k_x$
B ₁	<i>f</i> ₁ -wave	$\sin \frac{1}{2} k_y (\cos \frac{\sqrt{3}}{2} k_x - \cos \frac{1}{2} k_y)$
B ₂	<i>f</i> ₂ -wave	$\sin \frac{\sqrt{3}}{2} k_x (\cos \frac{\sqrt{3}}{2} k_x - \cos \frac{3}{2} k_y)$

Table I. Classification of the pairing symmetry in the triangular lattice. The first column shows the irreducible representations of D_6 group. The second column shows the notation adopted in this paper. The *s*-wave, *p*-wave, *etc* are the counterparts of the isotropic system. The third column shows the typical wave function of Cooper pairs.

Before showing the results, it is necessary to classify the pairing symmetry. The symmetry of Cooper pairs is classified into *s*-, *p*-, *d*-wave *etc.* in case of an isotropic system like ³He. For metals, the Cooper pairing is classified into the finite species according to the symmetry of crystals.⁴⁶⁾ We show the classification in case of the triangular lattice in Table I. We denote “*s*-wave”, “*d*-wave” *etc.* in analogy with the isotropic case. While the *s*-, *d*- and *i*-wave are spin singlet pairings, the *p*-, *f*₁- and *f*₂-wave are spin triplet pairings. Note that there remains two-fold degeneracy in the *p*- and *d*-wave states, namely p_x - and p_y -wave, d_{xy} - and $d_{x^2-y^2}$ -wave, respectively. The time-reversal-symmetry-breaking is expected below T_c in the *d*-wave state, as discussed in the RVB theory.²¹⁻²⁴⁾ On the contrary, time-reversal-symmetry is not necessarily broken in the *p*-wave case because there is an internal degree of freedom of the direction of $S = 1$, as discussed in Sr_2RuO_4 .³⁵⁾

The eigenvalues of the Éliashberg equation, eq. (17) are classified according to the symmetry of Cooper pairs. The pairing symmetry corresponding to the largest eigenvalue is stabilized below T_c . Hereafter, we ignore the possibility of *s*-wave pairing because the strong on-site repulsion will destabilize even the extended *s*-wave pairing. When the symmetry of crystal is lowered, some candidates in Table I are classified into the same irreducible representation. For example, the d_{xy} -wave and *s*-wave symmetries are included in the same representation for the anisotropic triangular lattice.^{47, 48)} However, we can ignore this possibility in the isotropic triangular lattice.

3.2 Phase diagram of three-orbital model

In order to search possible pairing symmetries in a phase diagram, we introduce two controlling parameters, a and n_e . Among the hopping matrix elements in eqs. (6–11), t_3 is fixed to 1 but the other matrix elements are chosen to be

$$(t_1, t_2, t_4, t_5, t_6, t_7, t_8, t_9) = \\ a(0.1, 0.2, 0.3, -0.2, -0.05, 0.2, 0.2, -0.25). \quad (19)$$

In case of $a = 0$, the system is regarded to be a superposition of kagome lattice,²⁰⁾ but we have to choose $a \geq 0.6$ in order to obtain a realistic Fermi surface. Although there are many choices of controlling the minor matrix elements, we have confirmed that the following results are qualitatively independent of the choice.

As another controlling parameter, we use the hole number n_e of the e_g -Fermi surface, which can be altered by adjusting the crystal field splitting e_c . When we decrease e_c , the energy of e_g -orbitals is lowered and thus n_e decreases. We have confirmed that the value n_e is essential rather than the total electron number n for the following results which are almost independent of the way to alter n_e . Note that the total electron number is fixed as $n = 5.33$ throughout this paper.

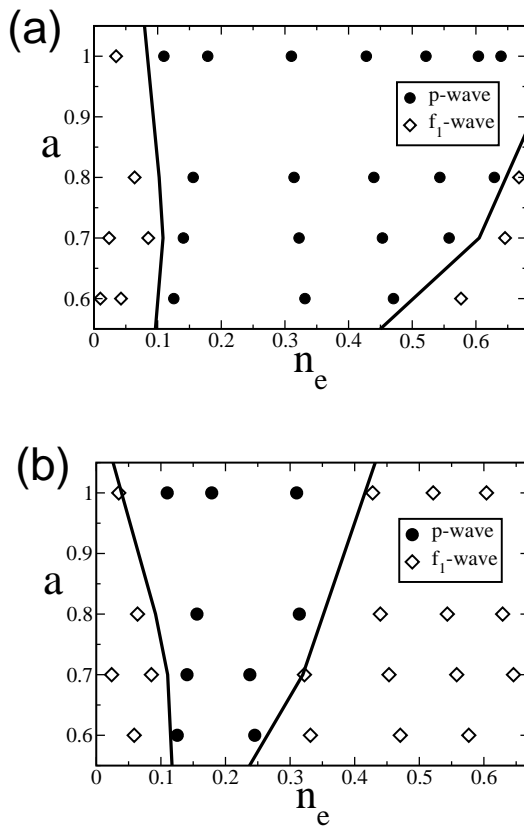


Fig. 3. Phase diagram for (a) $U' = J_H = J = U/3$ and (b) $U' = U/2$ and $J_H = J = U/4$. The horizontal axis describes the hole number included in the e_g -Fermi surface. The solid line is the phase boundary obtained by the interpolation.

Figure 3 shows the most stable pairing symmetry in the phase diagram of a and n_e for two values of the inter-

action strength. The temperature is fixed to be $T = 0.01$ and we divide the first Brillouin zone into 128×128 lattice points and take 512 Matsubara frequencies. We have confirmed that the obtained results do not depend on the numerical details, qualitatively.

We fix $U = 5$ and change the value of $J_H = J$. Under the reasonable conditions $U = U' + 2J_H$ and $U' - J_H > 0$, $J_H = U/3$ is the maximum value of the Hund's rule coupling. As shown in Fig. 3, the spin triplet p -wave superconductivity is widely stabilized at $J_H = U/3$. The f_1 -wave superconductivity is also stabilized when e_g -Fermi surface is very small or very large. For the values of n_e expected in the LDA calculation, namely $n_e = 0.1 \sim 0.4$, we obtain the p -wave superconductivity independent of the value of a . When the value of Hund's rule coupling is decreased (Fig. 3(b)), the f_1 -wave superconductivity becomes more stable. We see that in both cases the spin triplet superconductivity is stable.

Note that the e_g -Fermi surface vanishes in case of $n_e = 0$. Then, it is difficult to determine the pairing state since the tendency to superconductivity is very weak independent of the pairing symmetry. On the other hand, the superconductivity is not significantly affected by the disappearance of a_{1g} -Fermi surface which occurs at $n_e = 0.67$.

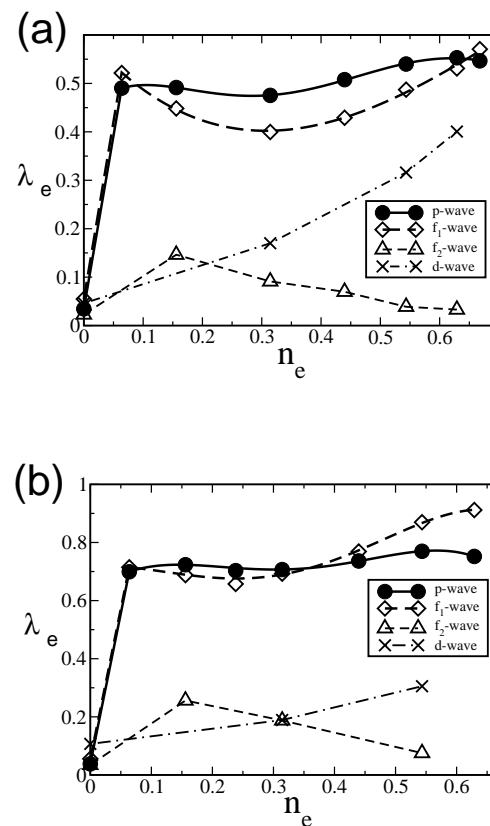


Fig. 4. n_e -dependence of eigenvalues of Éliashberg equation. We choose $a = 0.8$ and (a) $U' = J_H = J = U/3$, (b) $U' = U/2$ and $J_H = J = U/4$ at $T = 0.01$.

In order to make the situation clearer, we show the eigenvalues of Éliashberg equation for each pairing sym-

metry in Fig. 4. It is shown that the p - and f_1 -wave superconductivity give nearly degenerate eigenvalues in a wide parameter range. If we choose the weak crystal field splitting $e_c \sim 0$, we obtain $n_e \sim 0.3$ which is consistent with LDA calculation. The n_e -dependence of eigenvalue in the f_1 -wave symmetry shows a minimum in this region. As a result, the p -wave superconductivity is stable around this region. As the Hund's rule coupling decreases, the f_1 -wave state is stabilized more widely. The maximum eigenvalue increases with the decrease of Hund's rule coupling which leads to the enhancement of T_c (See also Fig. 6). Note that the eigenvalues for the d -wave, i -wave and f_2 -wave states are very small compared to the p - and f_1 -wave states. As is shown later, the d -wave state is stabilized when Hund's rule coupling is very small.

Another interesting result in Fig. 4 is that the maximum eigenvalue does not significantly depend on n_e . Even if the size of e_g -Fermi surface is remarkably reduced, the instability of superconductivity is not suppressed unless the e_g -Fermi surface vanishes. This is mainly because the DOS of e_g -Fermi surface little depends on the value n_e . This is one of the characteristics of the two-dimensional system in the low density region. Note that the number of hole included in each hole pocket is very small as $n_h/6 \sim 0.05$. Then, an analogy with the isotropic system like ^3He is partly justified. This picture is important for the pairing mechanism as we will explain in §3.3. The n_e -dependence of T_c can be measured by varying the Na-intercalation of $\text{Na}_x\text{CoO}_2 \cdot y\text{H}_2\text{O}$. However, experimental results are controversial.^{49,50)}

The eigenvalue rapidly decreases when e_g -Fermi surface vanishes. This result indicates that the e_g -Fermi surface plays an essential role for the superconductivity. This implication will be clearly confirmed in §4.2. Although the eigenvalues are very small at $n_e = 0$, the d -wave symmetry seems to be most stable. In this case, the topology of Fermi surface is equivalent to the simple triangular lattice including only the nearest neighbor hopping. This is consistent with the RVB theory based on the t - J model in the triangular lattice, which shows the $d_{x^2-y^2} \pm id_{xy}$ -wave superconductivity.²¹⁻²⁴⁾ However, the used parameters are quite different. The t - J model assumes $U/t > 8$, while $U/t = 5$ in this paper. In the intermediate coupling region, the momentum dependence arising from the vertex correction is probably important when the SOP gives very small λ_e .³³⁾ In case of the simple triangular lattice, the lowest order vertex correction favors the p -wave state.³⁹⁾ It should be stressed that the SOP gives much larger value of λ_e when e_g -Fermi surface exists, as shown in Fig. 4.

Fig. 5 shows the a -dependence of eigenvalues. It is shown that the eigenvalue monotonically increases with decreasing a . This variation is basically owing to the increase of the DOS. In case of $a = 0.5$, almost flat band is realized around the e_g -Fermi surface. Therefore, a steep increase of the eigenvalue leading to the remarkable enhancement of T_c occurs toward this region. We note that most important parameter for the appearance of flat band is the next nearest neighbor hoppings. Although by changing the parameter a , the nearest and third nearest

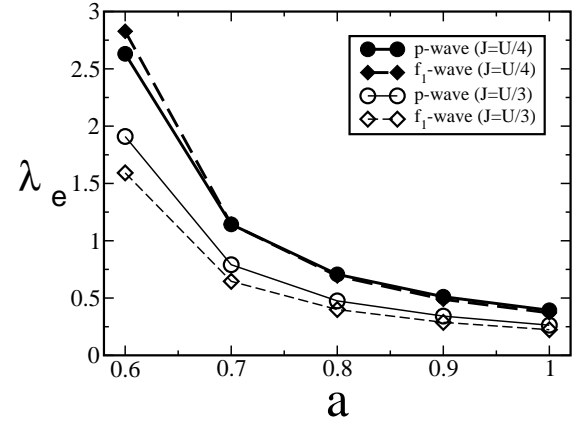


Fig. 5. a -dependence of eigenvalues of Éliashberg equation. We choose the parameter $J_H = U/3$ or $J_H = U/4$. Here, we fix the parameter $e_c = 0$ instead of n_e . Therefore, n_e slightly differs from $n_e = 0.33$ at $a = 0.6$ to $n_e = 0.31$ at $a = 1$.

neighbor hoppings vary simultaneously, these parameters play only quantitative roles. From Figs. 3-5, we can see that the variable a is important for the value of T_c , while the variable n_e plays an essential role for determining the pairing symmetry.

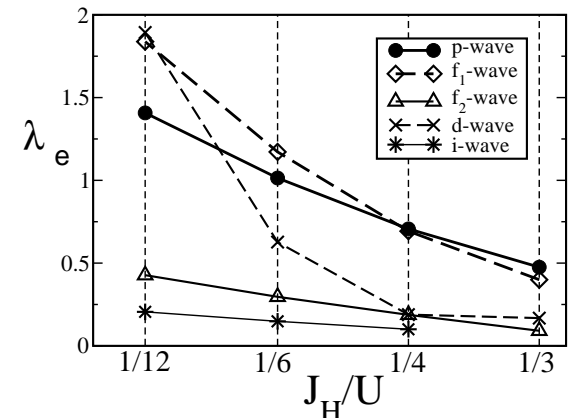


Fig. 6. J_H -dependence of eigenvalues of Éliashberg equation. The parameters are chosen to be $a = 0.8$ and $n_e = 0.31$.

Before closing this subsection, let us discuss the possibility of d -wave superconductivity in case of the small Hund's rule coupling. Fig. 6 shows the J_H -dependence of eigenvalues for each pairing symmetry. It is shown that all eigenvalues increase with the decrease of Hund's rule coupling. Among them, the eigenvalue in the d -wave symmetry increases most rapidly and the d -wave superconductivity is stabilized for $J_H < U/12$. The phase diagram in the J_H - n_e plane is shown in Fig. 7, where the d -wave superconductivity is more stabilized in the region with small value of n_e .

This stability of the d -wave pairing will be owing to the large value of U' which is comparable to U . The inter-orbital repulsion U' couples to the charge and orbital excitations which equivalently contribute to the effective interactions in the singlet and triplet channels. There-

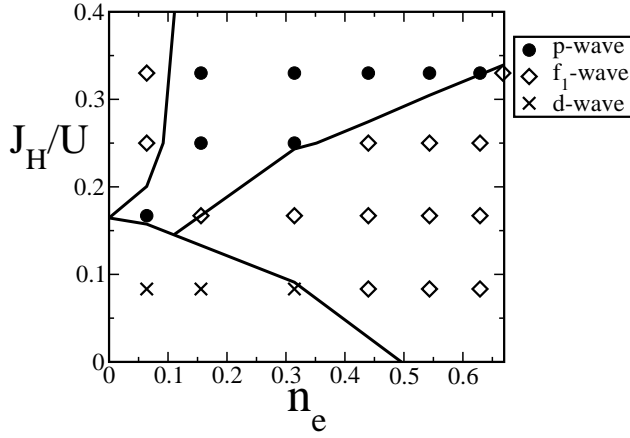


Fig. 7. Phase diagram in the J_H - n_e plane at $a = 0.8$. The solid line is the phase boundary obtained by the interpolation.

fore, the difference between singlet and triplet superconductivity is reduced when U' is large. In other words, the Hund's rule coupling favors the spin triplet superconductivity, although the value of T_c is reduced. However, higher order terms generally enhance the spin excitation which mostly couples to J_H and U . Therefore, we expect that the d -wave superconductivity is less stable if we include the higher order terms. This is confirmed from the FLEX calculation.⁴²⁾

3.3 Basic mechanism of superconductivity

In order to clarify the basic mechanism of superconductivity, we study the momentum dependence of effective interaction $V(k, k')$ in the spin triplet channel. Figure 8 shows the k' -dependence of $V(k, k')$ with \mathbf{k} being fixed at the momentum shown by an arrow at which the order parameter in the p -wave symmetry takes maximum value. It is apparent that there is a strong attractive interaction between momenta included in the same hole pocket Fermi surface. This is the reason why the spin triplet superconductivity is favored. We can show that in case of $J_H = U/3$, the effective interaction in the singlet channel has opposite sign to that in the triplet channel. This strong repulsive interaction suppresses the spin singlet superconductivity.

The microscopic origin of this momentum dependence can be understood as follows. First, we point out the ferromagnetic character of spin fluctuation. Fig. 9(a) shows the spin susceptibility which is estimated by the Kubo formula within the bubble diagram. We see that the spin susceptibility has a trapezoidal peak around $\mathbf{q} = 0$. Note that the ferromagnetic spin fluctuation has been expected in the LDA calculation⁴⁰⁾ and observed by the NMR.¹³⁾ Owing to the ferromagnetic character of spin susceptibility, the attractive interaction in the same hole pocket is very strong and favors the spin triplet superconductivity.

The ferromagnetic spin fluctuation is basically comes from the e_g -Fermi surface. As pointed out by Kuroki *et al.*,²⁸⁾ the van Hove singularity near the K points leads to a large DOS of e_g -Fermi surface. Then, each hole pocket gives rise to ferromagnetic spin fluctuation like in the

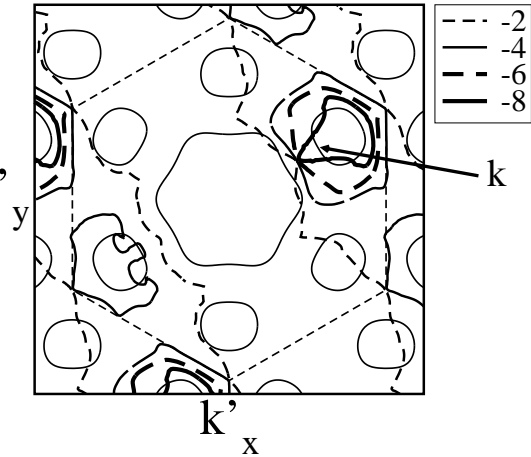


Fig. 8. Contour plot of the effective interaction $V(k, k')$. The initial momentum \mathbf{k} is shown in the figure. The horizontal and vertical axis show k'_x and k'_y , respectively. Matsubara frequency is fixed to the lowest value $\omega_n = \omega'_n = \pi T$. The Fermi surface is simultaneously described by the thin solid line. The parameters are chosen to be $n_e = 0.31$, $a = 0.8$, $U' = U/2$ and $J_H = J = U/4$.

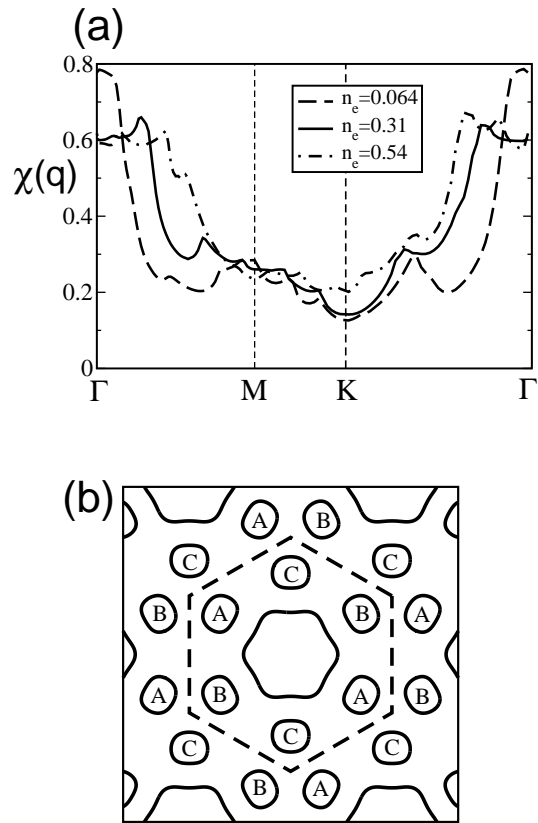


Fig. 9. (a) Momentum dependence of the static spin susceptibility at $a = 0.8$. (b) Schematic figure for the classification of hole pockets.

two-dimensional electron gas, which has a susceptibility with the trapezoidal structure. Actually, as shown in Fig. 9(a), when we increase the size of hole pockets by changing n_e , the width of the trapezoidal peak around the Γ point increases.

Here, we illuminate the essential roles of the orbital

degree of freedom. First, we point out that the ferromagnetic spin fluctuation is indeed induced by the orbital degree of freedom. In the multi-orbital model, the spin susceptibility is determined by the dispersion relation and the structure factor arising from the orbital degree of freedom. If we neglect the momentum dependence of structure factor as was done in the previous studies,^{29,51)} we obtain two peaks of spin susceptibility which are quite different from ours. One is located around the Γ point and the other is slightly removed from the Γ point. However, we obtain the trapezoidal peak centered at the Γ point by appropriately taking account of the structure factor. Thus, the frustration inherent in the triangular lattice is removed by the orbital degree of freedom which gives rise to the ferromagnetic spin fluctuation.

We point out that the roles of the orbital degree of freedom can be understood by considering the momentum dependence of the wave function which is expressed by the unitary matrix $\hat{U}(\mathbf{k})$ in eq. (15). This wave function indicates the orbital character of quasi-particles (see also §4). The structure factor of spin discussed above is also obtained by this wave function. Furthermore, the effective interaction $V(k, k')$ has another distinct property arising from this momentum dependence. As we have mentioned before, the e_g -Fermi surface mainly consists of the e_g -doublet whose wave function is shown in eqs. (12) and (13). Furthermore, we find that the six hole pockets are divided into three pairs as is shown in Fig. 9(b). For example, more than 90% of the weight of pair “A” originates from the orbital $|e_g, 1\rangle$, while the other two pairs are dominated by a linear combination of $|e_g, 1\rangle$ and $|e_g, 2\rangle$. It is generally expected that the electron correlation between the same orbitals is stronger than that between the different orbitals. Actually, the effective interaction between different pairs “A”, “B” and “C” is smaller than those between the same pairs, as shown in Fig. 8. This is the reason why the p - and f_1 -wave superconductivities are stabilized with nearly degenerate eigenvalues as shown in Fig. 4. Which is more stable between p - and f_1 -wave states depends on the coupling between different pairs of hole pockets, which is robustly small as explained above. Note that if we apply the phenomenological theory on the spin-fluctuation-induced superconductivity to $\text{Na}_x\text{CoO}_2 \cdot y\text{H}_2\text{O}$, the f_1 -wave superconductivity is widely stabilized. The single band model leading to the ferromagnetic spin fluctuation²⁸⁾ also expects the f_1 -wave symmetry. However, the p -wave superconductivity can be stabilized in the present case owing to the orbital degeneracy.

It should be noticed that the origin of trapezoidal peak of spin susceptibility around Γ point is clearly understood by this momentum dependence of wave function. Although the wave functions are not orthogonal between different pairs of hole pockets, the matrix elements between them in calculating $\chi(q)$ are small. Therefore, in the zeroth order approximation, pairs of hole pockets are regarded to be decoupled from each other. Then, each hole pocket induce the trapezoidal peak of $\chi(q)$ as in the two-dimensional electron gas model.

Another point to stabilize the superconductivity is the

disconnectivity of the e_g -Fermi surface as discussed before the discovery of $\text{Na}_x\text{CoO}_2 \cdot y\text{H}_2\text{O}$.³⁸⁾ Even in the anisotropic superconductivity of p -wave or f_1 -wave symmetry, the order parameter can take a same sign in each hole pocket, which stabilizes the superconductivity. Note that the difficulty of the paramagnon-induced-superconductivity (superfluidity) has been discussed for ^3He .⁵²⁾ This difficulty is removed by the topological aspect of Fermi surface in case of $\text{Na}_x\text{CoO}_2 \cdot y\text{H}_2\text{O}$.

3.4 Momentum dependence of superconducting gap

Next, we show the momentum dependence of order parameter $\Delta(\mathbf{k}, i\pi T)$ in Fig. 10. Although λ_e does not reach 1 at $T = 0.01$, it is generally expected that $\Delta(\mathbf{k}, i\pi T)$ shows the momentum dependence of superconducting gap below T_c . Note that even if the superconducting instability is dominated by the e_g -Fermi surface, the a_{1g} -Fermi surface also contributes to the observable quantities, such as NMR $1/T_1T$, specific heat and magnetic field penetration depth.

Fig. 10(a) shows the order parameter in the p -wave symmetry. We choose the Hund’s rule coupling as $J_H = U/3$ where the p -wave superconductivity is stabilized. Among the two degenerate p_x - and p_y -states, only the p_y -state is shown. Because of the discontinuity of the e_g -Fermi surface, the order parameter is node-less on the e_g -Fermi surface, while it has nodes on the a_{1g} -Fermi surface. Since $p_x\hat{x} \pm p_y\hat{y}$, $p_x\hat{y} \pm p_y\hat{x}$ or $(p_x \pm ip_y)\hat{z}$ states are expected below T_c , the superconducting gap becomes $\sqrt{\Delta_x(k)^2 + \Delta_y(k)^2}$, where $\Delta_x(k)$ and $\Delta_y(k)$ are the order parameters for p_x - and p_y -states, respectively. In this case, the superconducting gap does not vanish even on the a_{1g} -Fermi surface. But, we find a remarkable anisotropy of the superconducting gap on the a_{1g} -Fermi surface which can explain the power-law behaviors of NMR $1/T_1T$ and so on as in the case of Sr_2RuO_4 .⁵³⁾ However, we note that this is an accidental result.

Fig. 10(b) shows the order parameter in the f_1 -wave symmetry. We choose the Hund’s rule coupling as $J_H = U/6$ where the f_1 -wave superconductivity is most stable. We can see the clear six times alternation of the sign of order parameter. Also in this case, the e_g -Fermi surface is node-less and a_{1g} -Fermi surface has line nodes. As we showed before for the magnetic penetration depth,¹⁵⁾ the combination of fully gapped e_g -Fermi surface and line nodes on a_{1g} -Fermi surface gives an intermediate temperature dependence between s -wave and anisotropic superconductivity.

In Fig. 10(c) we show the order parameter in the d_{xy} -wave state which is stabilized when J_H is very small, $J_H = U/12$. The $d_{xy} \pm id_{x^2-y^2}$ state is expected below T_c and both a_{1g} -Fermi surface and e_g -Fermi surface are node-less in this case. The exponential behaviors in many quantities are expected unless some accidental situation occurs as in the p -wave state. Our calculation does not support such an accidental situation in the d -wave symmetry.

Note that in all of the above cases we have shown, the amplitude of order parameter is large on the e_g -Fermi surface, while it is small on the a_{1g} -Fermi surface. This result is expected from the fact that the e_g -Fermi surface

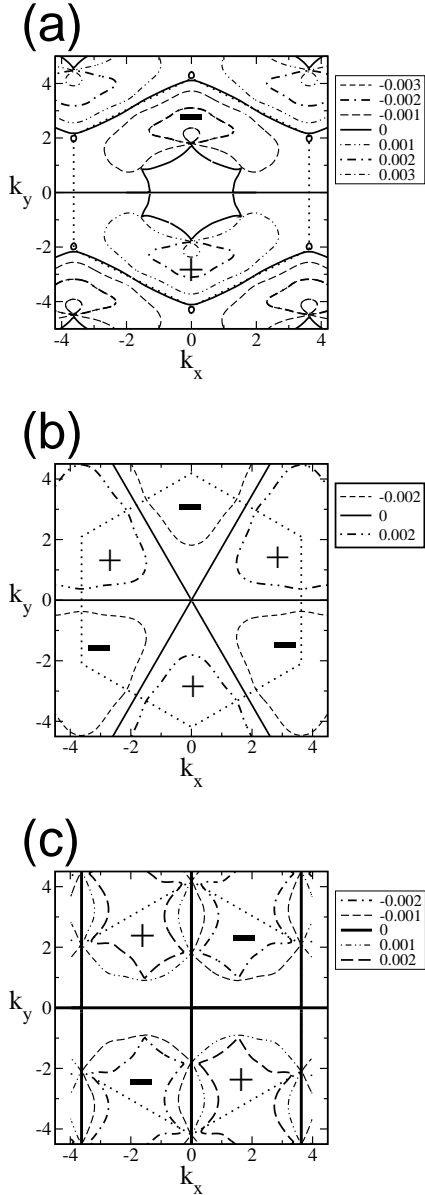


Fig. 10. Momentum dependence of order parameter (a) in the p_y -wave symmetry, (b) in the f_1 -wave symmetry and (c) in the d_{xy} -wave symmetry. The parameters are chosen to be $a = 0.8$ and $n_e = 0.31$.

is responsible for the pairing instability as discussed in §3.3. This point will be clarified in more details in the next section.

4. Reduced Models

We have analyzed the possibility of unconventional superconductivity in $\text{Na}_x\text{CoO}_2 \cdot y\text{H}_2\text{O}$ on the basis of the three-orbital model. Because calculations for this model need much computational time, a simplified model appropriate for studying the superconductivity is highly desired for a future development in the theoretical field. In this section, we try to find an appropriate model from the comparison to the three-orbital model. We show that the two-orbital model is satisfactory for this purpose, while the single-orbital model is not. The essential origin of the results in §3 will be clarified by these trials.

4.1 Failure of single-orbital Hubbard model

Thus far, we have stressed some essential roles of the orbital degeneracy. They are illuminated by showing the failure of single-orbital model. Some authors have already studied single band Hubbard models reproducing the LDA Fermi surface.^{28,29)} In this paper, we try a single band Hubbard model by keeping only the γ -band, *i.e.*, the highest-energy eigenstates obtained in eq. (15). Hamiltonian is expressed in the following way.

$$H_1 = \sum_{\mathbf{k},s} E_3(\mathbf{k}) c_{\mathbf{k},s}^\dagger c_{\mathbf{k},s} + U \sum_i n_{i,\uparrow} n_{i,\downarrow}. \quad (20)$$

As has been shown in Fig. 1, the typical Fermi surface is reproduced in this model. Indeed, this is the minimal model describing the electron correlation in this material. However, as shown below, this model is inappropriate for the superconductivity because the results are qualitatively different from those in the multi-orbital model.

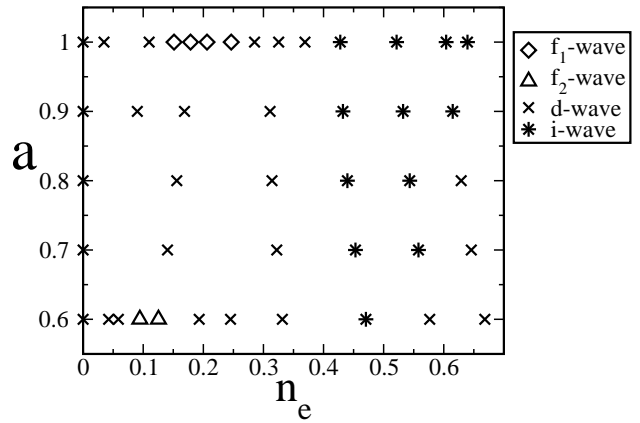


Fig. 11. Phase diagram of the single-orbital Hubbard model. The qualitatively different results from Fig. 3 indicate the failure of this model.

In Fig. 11, we show the phase diagram obtained by the SOP applied to the single band Hubbard model (eq. (20)). It is shown that the d -wave and i -wave superconductivities are widely stabilized instead of p -wave or f_1 -wave states. The f_1 -wave superconductivity competes with the d -wave one, but is stabilized only in a narrow region. On the other hand, the p -wave state which is stable in the multi-orbital model is not stabilized in the whole parameter space.

This difference arises from the disregard of the momentum dependence of wave function. If we neglect the momentum dependence of $\hat{U}(\mathbf{k})$ in eq. (15), the three-orbital model is exactly reduced to the single-orbital Hubbard model in eq. (20). The difference of stable pairing state is apparent if we check the spin susceptibility $\chi(q)$. In the single-orbital model, $\chi(q)$ is similar to that obtained in Ref. 29 and we do not clearly see the ferromagnetic tendency. As a result, the momentum dependence of the effective interaction is qualitatively different from that of three-orbital model.

This difference is partly improved by neglecting the a_{1g} -orbital like Ref. 28. However, the coupling between

different pairs of hole pockets stabilizes the f_1 -wave state much more than the p -wave state. This is inconsistent with the results in §3. In the multi-orbital model analyzed in §3, the character of orbital in each hole pocket Fermi surface induces the nearly degeneracy between p -wave and f_1 -wave states.

4.2 Effective two-orbital model

The results in the previous subsection show that the single-orbital Hubbard model is qualitatively inappropriate for studying the superconductivity. The important factor to be taken into account is the orbital character of quasi-particles on each Fermi surface. This is described by the momentum dependence of the unitary matrix $\hat{U}(\mathbf{k})$ in eq. (15). Considering these points, we propose an simplification of the three-orbital model in this subsection. The reduced model is an effective two-orbital model representing the e_g -doublet. The simplification is performed by the following two steps.

(1) The a_{1g} -orbital is simply ignored.

(2) The lower band below the Fermi level is ignored.

The first step is justified because we find that the superconducting instability is dominated by the six hole pockets which mainly consist of the e_g -orbitals. The second one is generally justified because the quasi-particles around the Fermi surface lead to the superconductivity.

In order to perform the first step, we transform the basis of local orbitals. This is carried out by using the unitary transformation as,

$$(d_{\mathbf{k},1,s}^\dagger, d_{\mathbf{k},2,s}^\dagger, d_{\mathbf{k},3,s}^\dagger) = (c_{\mathbf{k},1,s}^\dagger, c_{\mathbf{k},2,s}^\dagger, c_{\mathbf{k},3,s}^\dagger) \hat{U}_1, \quad (21)$$

$$\hat{U}_1 = \begin{pmatrix} \frac{1}{\sqrt{3}} & 0 & \frac{2}{\sqrt{6}} \\ \frac{\sqrt{1}}{\sqrt{3}} & \frac{1}{\sqrt{2}} & -\frac{1}{\sqrt{6}} \\ \frac{\sqrt{1}}{\sqrt{3}} & -\frac{1}{\sqrt{2}} & -\frac{1}{\sqrt{6}} \end{pmatrix}. \quad (22)$$

The interaction term H_1 in the Hamiltonian H_3 is invariant for this unitary transformation owing to the relations $U = U' + 2J_H$ and $J_H = J$. The non-interacting term is transformed as,

$$H_0 = \sum_{\mathbf{k},s} d_{\mathbf{k},s}^\dagger \hat{H}'(\mathbf{k}) d_{\mathbf{k},s}, \quad (23)$$

$$\hat{H}'(\mathbf{k}) = \hat{U}_1^\dagger \hat{H}(\mathbf{k}) \hat{U}_1. \quad (24)$$

The first step is performed by dropping the creation (annihilation) operator $d_{\mathbf{k},1,s}^\dagger$ ($d_{\mathbf{k},1,s}$) which corresponds to the a_{1g} -orbital. As a result, the three-orbital model is reduced to the following two-orbital model.

$$\begin{aligned} H_2 = & \sum_{\mathbf{k},s} a_{\mathbf{k},s}^\dagger \hat{h}(\mathbf{k}) a_{\mathbf{k},s} + U \sum_i \sum_{a=1}^2 n_{i,a,\uparrow} n_{i,a,\downarrow} \\ & + U' \sum_i \sum_{a>b} n_{i,a} n_{i,b} - J_H \sum_i \sum_{a>b} (2S_{i,a} S_{i,b} + \frac{1}{2} n_{i,a} n_{i,b}) \\ & + J \sum_i \sum_{a \neq b} a_{i,a,\downarrow}^\dagger a_{i,a,\uparrow}^\dagger a_{i,b,\uparrow} a_{i,b,\downarrow}. \end{aligned} \quad (25)$$

Here, we have introduced a 2×2 matrix $\hat{h}(\mathbf{k})_{i,j} = \hat{H}'(\mathbf{k})_{i+1,j+1}$ and two component vector $a_{\mathbf{k},s}^\dagger =$

$(d_{\mathbf{k},2,s}^\dagger, d_{\mathbf{k},3,s}^\dagger)$. Then, the Green function is described by a 2×2 matrix as $\hat{G}(\mathbf{k}) = (i\omega_n \hat{1} - \hat{h}(\mathbf{k}))^{-1}$, which is expressed as

$$G_{ij}(k) = \sum_{\alpha=1}^2 v_{i\alpha}(\mathbf{k}) v_{j\alpha}(\mathbf{k}) G_\alpha(k). \quad (26)$$

Here, $v_{i\alpha}(\mathbf{k})$ are components of the unitary matrix $\hat{V}^\dagger(\mathbf{k})$ which diagonalizes the matrix $\hat{h}(\mathbf{k})$

$$\hat{V}^\dagger(\mathbf{k}) \hat{h}(\mathbf{k}) \hat{V}(\mathbf{k}) = \begin{pmatrix} e_1(\mathbf{k}) & 0 \\ 0 & e_2(\mathbf{k}) \end{pmatrix}, \quad (27)$$

with $e_1(\mathbf{k}) < e_2(\mathbf{k})$. The diagonalized Green function is obtained as $G_\alpha(k) = \frac{1}{i\omega_n - e_\alpha(\mathbf{k})}$.

We show the dispersion relation $e_1(\mathbf{k})$ and $e_2(\mathbf{k})$ in Fig. 12. Apparently the band structure around the e_g -Fermi surface is reproduced by this simplification, while the a_{1g} -Fermi surface vanishes.

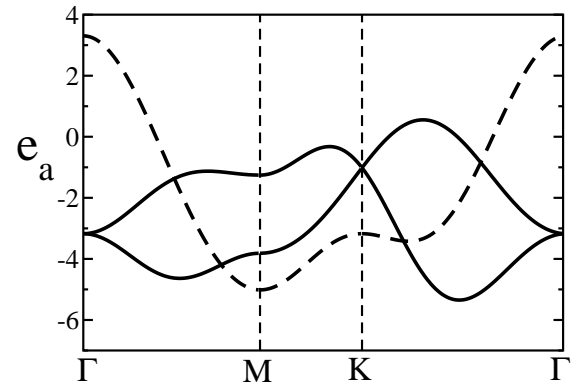


Fig. 12. Dispersion relation in the two-orbital model (solid lines). The parameters are chosen to be $a = 0.8$ and $n_e = 0.36$. We have shown the dispersion relation of the a_{1g} -orbital which is obtained as $\hat{H}'(\mathbf{k})_{11} - \mu$ (dashed line).

The second step is performed by ignoring the lower energy band, $e_1(\mathbf{k})$. Then, the Green function is obtained as, $G_{ij}(k) = v_{i2}(\mathbf{k}) v_{j2}(\mathbf{k}) G_2(k)$. Owing to this procedure, the calculation becomes equivalent to that for a single band Hamiltonian with momentum-dependent interaction,

$$\begin{aligned} H_L = & \sum_{\mathbf{k},s} e_2(\mathbf{k}) c_{\mathbf{k},s}^\dagger c_{\mathbf{k},s} \\ & + \sum_{\mathbf{q},\mathbf{k}',\mathbf{k}} S(\mathbf{q},\mathbf{k}',\mathbf{k}) c_{\mathbf{q}-\mathbf{k},\uparrow}^\dagger c_{\mathbf{q}-\mathbf{k}',\downarrow}^\dagger c_{\mathbf{k}',\downarrow} c_{\mathbf{k},\uparrow} \\ & + \sum_{\mathbf{q},\mathbf{k}',\mathbf{k},\sigma} S'(\mathbf{q},\mathbf{k}',\mathbf{k}) c_{\mathbf{q}-\mathbf{k},\sigma}^\dagger c_{\mathbf{q}-\mathbf{k}',\sigma}^\dagger c_{\mathbf{k}',\sigma} c_{\mathbf{k},\sigma}. \end{aligned} \quad (28)$$

The momentum dependent factors $S(\mathbf{q},\mathbf{k}',\mathbf{k})$ and $S'(\mathbf{q},\mathbf{k}',\mathbf{k})$ are expressed by the Coulomb interactions U , U' , J_H and J and the wave function $v_{i2}(\mathbf{k})$. If we neglect the momentum dependence of unitary matrix $\hat{V}^\dagger(\mathbf{k})$, the factor $S(\mathbf{q},\mathbf{k}',\mathbf{k})$ becomes U and $S'(\mathbf{q},\mathbf{k}',\mathbf{k}) = 0$. Then, the model is reduced to the single-orbital Hubbard model described by eq. (20) with use of $e_2(\mathbf{k})$ instead of $E_3(\mathbf{k})$.

We have discussed in §4.1 that this single-orbital Hubbard model is not appropriate. We show that the Hamiltonian H_L in eq. (28) with effective long range interaction is appropriate.

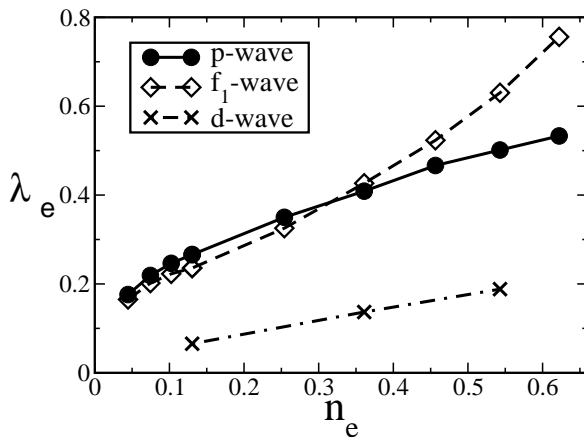


Fig. 13. Eigenvalues of Éliashberg equation obtained in the effective two-orbital model. We choose the parameters $a = 0.8$ and $J_H = U/4$.

Fig. 13 shows the results for the simplified model, H_L . We show the n_e -dependence of the eigenvalues of Éliashberg equation. The increase of eigenvalues with n_e is steeper than that in Fig. 4. This is mainly owing to the increase of DOS. However, the relation between each pairing symmetry closely resembles. For example, the p -wave superconductivity is stable around $n_e = 0.2$, while the f_1 -wave superconductivity is realized for larger values of n_e . The eigenvalue for the spin singlet d -wave superconductivity is far below that for the spin triplet one. This shows that the effective two-orbital model described by eq. (25) or eq. (28) reproduces the results in §3. The fact that the step (1) is appropriate clearly means that the superconductivity is basically led by the e_g -Fermi surface. The a_{1g} -Fermi surface plays only a secondary role.

Note that the step (1) decreases the eigenvalue of Éliashberg equation, mainly because of the decreased DOS in the e_g -Fermi surface. We have confirmed that the step (2) slightly enhances the spin triplet superconductivity.

5. Effects of Vertex Corrections in a Two-Orbital Model

In this section, we study the effects of vertex corrections. Although it is desirable to study these effects in the three-orbital model, we use the effective two-orbital model whose validity has been demonstrated in §4.2, because of numerical difficulties. Generally speaking, the higher order terms may play an important role for the superconducting instability, since it is considered that most of unconventional superconductors are in the intermediate coupling region. For example, vertex correction which is not included in the RPA plays an important role to stabilize the spin triplet pairing in Sr_2RuO_4 .³⁴⁾

Therefore, it is an important issue to investigate the role of higher order corrections in the present model.

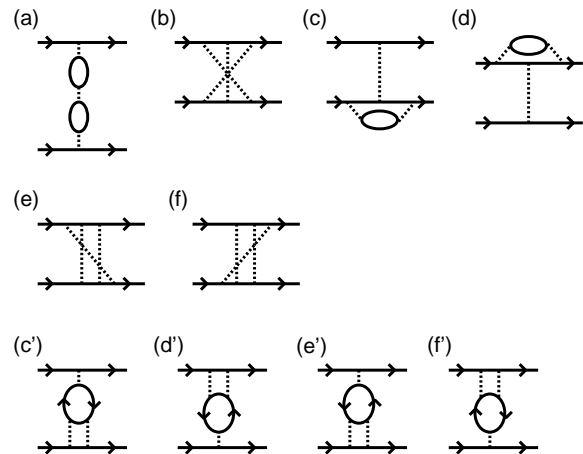


Fig. 14. Diagrammatic representation of the third order terms in the effective interaction. (a-f) correspond to the singlet channel or triplet channel with $d \parallel z$. (c'-f') correspond to the triplet channel with $d \perp z$.

We apply the third order perturbation theory (TOP) and its renormalized version to the Hamiltonian H_2 (eq. (25)) instead of H_L (eq. (28)). The parameter is chosen to be $J_H = U/3$, where the interaction between electrons with same spin vanishes and thus the number of diagrams is much reduced. As discussed in §3.2, this region will be relevant rather than the region where the Hund's rule coupling is small.

Fig. 14 shows the diagrammatic representation of third order terms in the effective interaction. Figs. 14(a) and (b) are classified into the RPA terms and others are the vertex corrections. The present theory is invariant for the rotation of spin, since we do not take account of the spin-orbit interaction. Therefore, the result on the spin triplet pairing does not depend on the direction of d -vector. Note that two RPA terms cancel each other in case of the spin triplet pairing with $d \parallel z$.

We numerically solve the Eliashberg equation within the TOP and show the eigenvalues in Fig. 15. We see that the p - and f_2 -wave superconductivity are significantly stabilized for $U > 4$, while the f_1 -wave and spin singlet pairings are unfavored. However, as discussed below, we find that these results in the intermediate coupling region are fictitious. Within the third order terms in Fig. 14, dominant contributions for triplet channel come from the terms represented in Figs. 14(e') and (f'), which include a particle-particle ladder. In contrast, the terms represented in Figs. 14(c') and (d') with a particle-hole ladder are negligible. As is well known in the Kanamori theory on the metallic ferromagnetism,⁵⁴⁾ the particle-particle ladder diagrams generally induce the screening of interaction as $U \rightarrow U(q) = U/(1 + U\phi(q))$ where $\phi(q)$ is obtained by the particle-particle ladder diagram. If q -dependence of $U(q)$ is not important, this scattering process is incorporated by the renormalized coupling constant \bar{U} . In the above TOP calculation, only the lowest

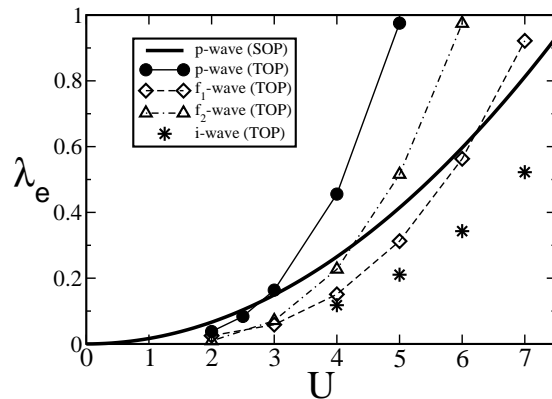


Fig. 15. Eigenvalues of Éliashberg equation in the third order perturbation theory. The thick solid line shows the maximum eigenvalue in the second order perturbation theory, which is classified into the p -wave symmetry. We do not show the eigenvalue in the d -wave symmetry because the tendency to superconductivity is very weak. We fix the parameters $a = 0.6$, $n_e = 0.35$ and $J_H = U/3$.

order term in the Kanamori-type correction was taken into account. Therefore, it is reasonable to think that the contributions from Figs. 14(e') and (f') can be suppressed if we include the higher order perturbation terms.

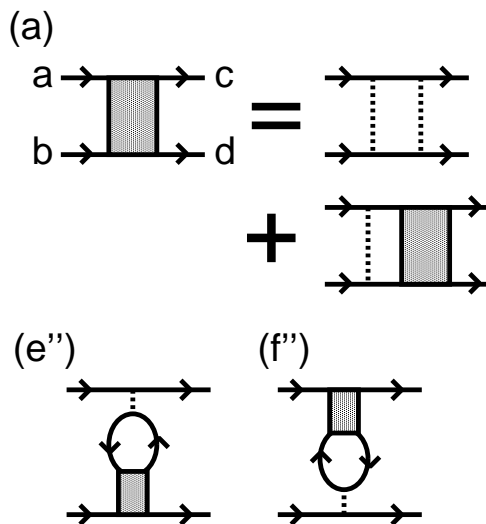


Fig. 16. (a) Renormalization of the particle-particle ladder diagram. In (e'') and (f''), the renormalized particle-particle ladder is used instead of bare ladder. In the RTOP, we take account of the terms (e'') and (f'') instead of (e') and (f') in Fig. 14.

In order to investigate this possibility, we perform a calculation of a renormalized TOP (RTOP), as shown in Fig. 16. The particle-particle ladder in Figs. 14(e') and (f') are replaced by the T-matrix shown in Fig. 16(a). As a result, the infinite order terms representing the screening effect are taken into account as in the Kanamori theory. By using the diagrams in Figs. 2, 14(c',d') and 16(e'',f''), we estimate the effective interaction and solve the Eliashberg equation. The obtained eigenvalues are shown in Fig. 17. It is apparent that the results of naive

TOP is significantly altered by the renormalization and that the correction to the SOP is small. In particular, the p -wave superconductivity is slightly stable over the f_1 -wave superconductivity. The nearly degeneracy between these states is also reproduced. The order parameter in each pairing symmetry is very similar to Fig. 10, although that in the naive TOP is remarkably different. We see that the eigenvalues are slightly reduced from the SOP, however the U -dependence is almost unchanged. These results are naturally interpreted if we consider that the vertex corrections basically work as a screening effect. Then, the second order perturbation theory is justified by regarding the interactions to be the renormalized ones.

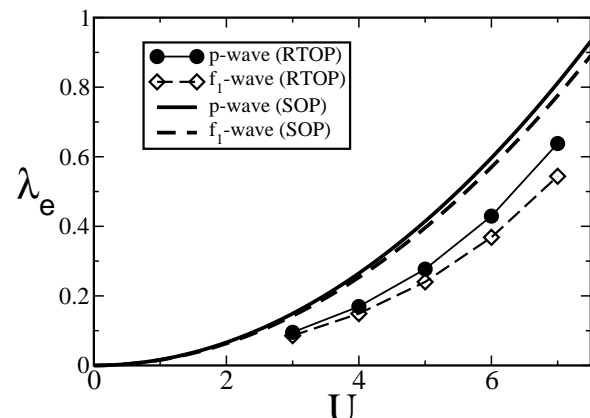


Fig. 17. Eigenvalues of Éliashberg equation in the renormalized third order perturbation theory for p -wave (circles) and f_1 -wave (diamonds) symmetry. Note that the eigenvalue in the f_2 -wave symmetry is very small. The thick solid and dashed lines show the eigenvalues in the second order perturbation theory for the p -wave and f_1 -wave symmetry, respectively. The parameters are the same as in Fig. 15.

Let us compare the present results to the case of high- T_c cuprates and Sr_2RuO_4 . For high- T_c cuprates, the d -wave superconductivity is basically induced by the RPA terms and the vertex correction due to the particle-particle ladder diagrams effectively reduces the coupling constant.^{33,55)} Therefore, the situation is very similar to the present case, although there is a difference of singlet and triplet pairing. On the other hand, in case of Sr_2RuO_4 , the effective interaction derived from the RPA terms has very weak momentum dependence, which does not work for the anisotropic pairing. However, the q -dependence of particle-particle ladder in TOP favors the spin triplet superconductivity.³⁴⁾ Then, the naive discussion on the screening effect can not be applied. It has been confirmed that the qualitative results of TOP applied to Sr_2RuO_4 are not altered even when the renormalization of particle-particle ladder is taken into account.⁵⁶⁾ Thus, the basic mechanism of possible spin triplet superconductivity in $\text{Na}_x\text{CoO}_2 \cdot y\text{H}_2\text{O}$ is qualitatively different from that in Sr_2RuO_4 .

6. Discussions

In this paper, we have investigated the multi-orbital model for $\text{Na}_x\text{CoO}_2 \cdot y\text{H}_2\text{O}$ on the basis of the perturbation theory. The obtained results indicate a possibility of spin triplet superconductivity in this material, although the *d*-wave superconductivity is also stabilized in a part of parameter space. There are two candidates of spin triplet pairing; *p*-wave and *f*-wave superconductivity are nearly degenerate.

Although the spin triplet superconductivity is one of the most interesting issues in the condensed matter physics, the microscopic theory remains in the developing stage. This is mainly owing to very few *d*-electron materials showing the spin triplet superconductivity. Although we see many candidates in the heavy fermion materials, the theoretical treatment is generally difficult for *f*-electron systems. Therefore, a discovery of spin triplet superconductor in transition metal oxides will lead to an important development in the microscopic understandings.

Probably, most established spin triplet superconductor in *d*-electron systems is Sr_2RuO_4 .³²⁾ Therefore, we have provided detailed discussions on the comparison between Sr_2RuO_4 and $\text{Na}_x\text{CoO}_2 \cdot y\text{H}_2\text{O}$. According to the results in this paper, $\text{Na}_x\text{CoO}_2 \cdot y\text{H}_2\text{O}$ provides a qualitatively different example from Sr_2RuO_4 in the following two points.

First, the RPA terms give rise to the dominant scattering process leading to the spin triplet pairing. The spin excitation is clearly ferromagnetic and favorable for the spin triplet pairing. This is in sharp contrast to the case of Sr_2RuO_4 where the vertex corrections are essential for the *p*-wave pairing. In case of $\text{Na}_x\text{CoO}_2 \cdot y\text{H}_2\text{O}$, the vertex corrections give rise to the screening effect which is not important for the qualitative results. While the ferromagnetic spin fluctuation-induced spin triplet superconductivity has been discussed from early years, the corresponding superconductivity has not been established until now. We expect that $\text{Na}_x\text{CoO}_2 \cdot y\text{H}_2\text{O}$ will be a first example realizing this mechanism.

Second, the orbital degeneracy plays an essential role in case of $\text{Na}_x\text{CoO}_2 \cdot y\text{H}_2\text{O}$. The conduction band in $\text{Na}_x\text{CoO}_2 \cdot y\text{H}_2\text{O}$ as well as that in Sr_2RuO_4 are basically described by three *t*_{2g}-orbitals. Although the single band Hubbard model is an appropriate model for describing the pairing mechanism of Sr_2RuO_4 ,³⁴⁾ such a simplification is qualitatively inappropriate for $\text{Na}_x\text{CoO}_2 \cdot y\text{H}_2\text{O}$. The success of single band Hubbard model for Sr_2RuO_4 is due to the electronic structure where the γ -band is basically described by the local *d*_{xy}-orbital. The failure for $\text{Na}_x\text{CoO}_2 \cdot y\text{H}_2\text{O}$ is due to the fact that the *e*_g-Fermi surface can not be described by any individual local orbital. In other words, the hybridization term in the unperturbed Hamiltonian is large in case of $\text{Na}_x\text{CoO}_2 \cdot y\text{H}_2\text{O}$, while it is negligible in Sr_2RuO_4 owing to the particular crystal symmetry. In this sense, the result on $\text{Na}_x\text{CoO}_2 \cdot y\text{H}_2\text{O}$ will be more general. Then, the momentum dependence of the wave function of quasi-particles essentially affects on the effective interaction leading to the Cooper pairing.

We have pointed out that the reduced two-orbital model is appropriate, instead of the failure of single-orbital model. This is because the Fermi surface in $\text{Na}_x\text{CoO}_2 \cdot y\text{H}_2\text{O}$ can be classified according to the local orbitals. Then, the superconductivity is basically triggered by the *e*_g-Fermi surface. Since a portion of *a*_{1g}-orbital in the *e*_g-Fermi surface is less than 5%, this orbital is safely ignored. This situation is similar to the case of Sr_2RuO_4 . However, the orbital degeneracy in *e*_g-doublet can not be ignored in the present case.

From the above comparisons, we obtain the following empirical rules.

(1) When the RPA-terms are favorable for the anisotropic superconductivity, the non-RPA terms are not qualitatively important, and *vice versa*.

(2) When a part of Fermi surface is described by a few local orbitals, the simplification of microscopic model is possible.

In particular, the second point will be helpful for a future development of microscopic understanding on multi-band superconductors. For example, several Fermi surfaces appear in heavy fermion materials. This fact as well as the 14-fold degeneracy in *f*-shell make the microscopic treatment difficult. However, it will be possible to obtain a simplified model by identifying the microscopic character of each Fermi surface.

Thus far, we have discussed the superconductivity in $\text{Na}_x\text{CoO}_2 \cdot y\text{H}_2\text{O}$ induced by the electron-electron correlation and highlighted the possibility of spin triplet pairing. However, clear experimental evidences for the symmetry of Cooper pairs have not been obtained up to now. Instead, we see some experimental observations which restrict the pairing state. For example, the absence of (or very small) coherence peak in NMR $1/T_1T$,¹⁰⁻¹³⁾ power-law temperature dependence of $1/T_1T$,^{12, 13)} NMR Knight shift below T_c ,^{10, 11, 57, 58)} and time-reversal symmetry observed in μSR ¹⁴⁾ should be cited, although a part of them are controversial. As for the results in this paper, spin triplet *p*- or *f*₁-wave superconductivity is consistent with the absence of coherence peak and with the power-law behaviors below T_c . In both cases, the (quasi-)line nodes appear in the *a*_{1g}-Fermi surface. In case of the *p*-wave pairing, the time-reversal-symmetry observed in μSR indicates a *d*-vector parallel to the plane, namely $p_x\hat{x} \pm p_y\hat{y}$ or $p_x\hat{y} \pm p_y\hat{x}$. This direction of *d*-vector is consistent with the recent measurements of NMR Knight shift under the parallel field^{11, 57, 58)} as well as macroscopic H_{c2} .^{7, 59)} These observations are consistent with the spin triplet superconductivity by assuming that the *d*-vector is strongly fixed against the applied magnetic field. Although we have shown that the anisotropy of *d*-vector in Sr_2RuO_4 is very small,³⁵⁾ this is partly owing to the particular electronic structure of Sr_2RuO_4 , and therefore we expect that the anisotropy is larger for $\text{Na}_x\text{CoO}_2 \cdot y\text{H}_2\text{O}$. The symmetry breaking interaction leading to the anisotropy arises from the second order term with respect to the spin-orbit interaction for Sr_2RuO_4 , while it arises from the first order term in case of $\text{Na}_x\text{CoO}_2 \cdot y\text{H}_2\text{O}$. Quantitative estimations for the anisotropy will be one of the interesting future issues.

On the other hand, the result of Knight shift indicates a spin singlet pairing if the symmetry breaking interaction is small. Then, the absence of time-reversal symmetry breaking will be a challenge for *d*-wave pairing because the $d_{x^2-y^2} \pm id_{xy}$ state is expected. The local distortion of triangular lattice, and the feedback effect will be candidates of the resolution. It seems that the *i*-wave superconductivity⁶⁰⁾ is consistent with the present experimental results except for the very weak impurity effects.⁶¹⁾ However, the microscopic mechanism leading to the pairing with $T_c = 5\text{K}$ will be difficult for such a high angular momentum state. In our study, we have not found the stable *i*-wave state. Although the observed impurity effect seems to support the *s*-wave pairing which is robust for the disorder, very short quasi-particle life time has to be assumed for the absence of coherence peak in $1/T_1T$. We consider that further vigorous investigations are highly desired for the identification of pairing state in $\text{Na}_x\text{CoO}_2 \cdot y\text{H}_2\text{O}$.

Acknowledgments

The authors are grateful to K. Ishida, Y. Kitaoka, Y. Kobayashi, M. Sato, Y. Tanaka and G.-q. Zheng for fruitful discussions. Numerical computation in this work was partly carried out at the Yukawa Institute Computer Facility. The present work was partly supported by a Grant-In-Aid for Scientific Research from the Ministry of Education, Science, Sports and Culture, Japan.

- 1) J. G. Bednorz and K. A. Müller, *Z. Phys. B* **64** (1986) 189.
- 2) F. Steglich, J. Aarts, C. D. Bredl, W. Lieke, D. Meschede, W. Franz, H. Schäfer, *Phys. Rev. Lett.* **43** (1979) 1892.
- 3) K. Takada, H. Sakurai, E. Takayama-Muromachi, F. Izumi, R. A. Dilanian and T. Sasaki, *Nature* **422** (2003) 53.
- 4) T. Motohashi, R. Ueda, E. Naujalis, T. Tojo, I. Terasaki, T. Atake, M. Karppinen, H. Yamauchi, *Phys. Rev. B* **67** (2003) 64406.
- 5) M. L. Foo, Y. Wang, S. Watauchi, H. W. Zandbergen, T. He, R. J. Cava and N. P. Ong, *Phys. Rev. Lett.* **92** (2004) 247001.
- 6) J. Sugiyama, H. Itahara, J. H. Brewer, E. J. Ansaldo, T. Motohashi, M. Karppinen and H. Yamauchi, *Phys. Rev. B* **67** (2003) 214420; J. Sugiyama, J. H. Brewer, E. J. Ansaldo, B. Hitti, M. Mikami, Y. Mori and T. Sasaki, *Phys. Rev. B* **69** 214423; J. Sugiyama, J. H. Brewer, E. J. Ansaldo, H. Itahara, T. Tani, M. Mikami, Y. Mori, T. Sasaki, S. Hebert and A. Maignan, *Phys. Rev. Lett.* **92** (2004) 017602.
- 7) F. C. Chou, J. H. Cho, P. A. Lee, E. T. Abel, K. Matan and Y. S. Lee, *Phys. Rev. Lett.* **92** (2004) 157004.
- 8) S. Y. Li, L. Taillefer, D. G. Hawthorn, M. A. Tanatar, J. Paglione, M. Sutherland, R. W. Hill, C. H. Wang and X. H. Chen, cond-mat/0401099.
- 9) K. Miyoshi, E. Morikuni, K. Fujiwara, J. Takeuchi and T. Hamasaki, *Phys. Rev. B* **69** (2004) 132412.
- 10) T. Waki, C. Michioka, M. Kato, K. Yoshimura, K. Takada, H. Sakurai and E. Takayama-Muromachi, cond-mat/0306036; C. Michioka, M. Kato, K. Yoshimura, K. Takada, H. Sakurai, E. Takayama-Muromachi and T. Sasaki, cond-mat/0403293.
- 11) Y. Kobayashi, M. Yokoi and M. Sato, *J. Phys. Soc. Jpn.* **72** (2003) 2161; 2453.
- 12) T. Fujimoto, G.-Q. Zheng, Y. Kitaoka, R. L. Meng, J. Cmaidalka and C. W. Chu, *Phys. Rev. Lett.* **92** (2004) 047004.
- 13) K. Ishida, Y. Ihara, Y. Maeno, C. Michioka, M. Kato, K. Yoshimura, K. Takada, T. Sasaki, H. Sakurai and E. Takayama-Muromachi, *J. Phys. Soc. Jpn.* **72** (2003) 3041; Y. Ihara, K. Ishida, C. Michioka, M. Kato, K. Yoshimura, K. Takada, T. Sasaki, H. Sakurai and E. Takayama-Muromachi, cond-mat/0407192.
- 14) W. Higemoto, K. Ohishi, A. Koda, R. Kadono, K. Ishida, K. Takada, K. Sakurai, E. Takayama-Muromachi and T. Sasaki, cond-mat/0310324.
- 15) Y. J. Uemura, P. L. Russo, A. T. Savici, C. R. Wiebe, G. J. MacDougall, G. M. Luke, M. Mochizuki, Y. Yanase, M. Ogata, M. L. Foo and R. J. Cava, cond-mat/0403031.
- 16) A. Kanigel, A. Keren, L. Patlagan, K. B. Chashka, P. King and A. Amato, *Phys. Rev. Lett.* **92** (2004) 257007.
- 17) H. D. Yang, J.-Y. Lin, C. P. Sun, Y. C. Kang, K. Takada, T. Sasaki, H. Sakurai and E. Takayama-Muromachi, cond-mat/0308031.
- 18) B. Lorenz, J. Cmaidalka, R. L. Meng and C. W. Chu, *Physica C* **402** (2004) 106.
- 19) A. Tanaka and X. Hu, *Phys. Rev. Lett.* **91** (2003) 257006.
- 20) W. Koshihara and S. Maekawa, *Phys. Rev. Lett.* **91** (2003) 257003.
- 21) G. Baskaran, *Phys. Rev. Lett.* **91** (2003) 097003; D. Sa, M. Sardar and G. Baskaran, cond-mat/0309563.
- 22) B. Kumar and B. S. Shastry, *Phys. Rev. B* **68** (2003) 104508; *Phys. Rev. B* **69** (2004) 059901(E).
- 23) Q.-H. Wang, D.-H. Lee and P. A. Lee, *Phys. Rev. B* **69** (2003) 092504.
- 24) M. Ogata, *J. Phys. Soc. Jpn.* **72** (2003) 1839.
- 25) C. Honerkamp, *Phys. Rev. B* **68** (2003) 68.
- 26) H. Ikeda, Y. Nisikawa and K. Yamada, *J. Phys. Soc. Jpn.* **73** (2004) 17.
- 27) Y. Tanaka, Y. Yanase and M. Ogata, *J. Phys. Soc. Jpn.* **73** (2004) 319.
- 28) K. Kuroki, Y. Tanaka and R. Arita, cond-mat/0311619.
- 29) Y. Nisikawa, H. Ikeda and K. Yamada, *J. Phys. Soc. Jpn.* **73** (2004) 1127.
- 30) O. I. Motrunich and P. A. Lee, *Phys. Rev. B* **69** (2004) 214516; cond-mat/0401160.
- 31) Y. Ando, N. Miyamoto, K. Segawa, T. Kawata and I. Terasaki, *Phys. Rev. B* **60** (1999) 10580.
- 32) Y. Maeno, H. Hashimoto, K. Yoshida, S. NishiZaki, T. Fujita, J. G. Bednorz and F. Lichtenberg, *Nature* **372** (1994) 532.
- 33) Y. Yanase, T. Jujo, T. Nomura, H. Ikeda, T. Hotta and K. Yamada, *Phys. Rep.* **387** (2004) 1.
- 34) T. Nomura and K. Yamada, *J. Phys. Soc. Jpn.* **69** (2000) 3678; *J. Phys. Soc. Jpn.* **71** (2002) 1993.
- 35) Y. Yanase and M. Ogata, *J. Phys. Soc. Jpn.* **72** (2003) 673.
- 36) T. Moriya and K. Ueda, *Adv. Phys.* **49** (2000) 555.
- 37) M. Vojta and E. Dagotto, *Phys. Rev. B* **59** (1999) R713.
- 38) K. Kuroki and A. Arita, *Phys. Rev. B* **63** (2001) 174507; *Phys. Rev. B* **64** (2001) 024501.
- 39) Y. Nisikawa and K. Yamada, *J. Phys. Soc. Jpn.* **71** (2002) 2629.
- 40) D. J. Singh, *Phys. Rev. B* **61** (2000) 13397; **68** (2003) 020503; M. D. Johannes and D. J. Singh, cond-mat/0401646.
- 41) J. Kuneš, K.-W. Lee and W. E. Pickett, cond-mat/0308388; K.-W. Lee, J. Kuneš and W. E. Pickett, cond-mat/0403018.
- 42) M. Mochizuki, Y. Yanase and M. Ogata, cond-mat/0407094.
- 43) M. Z. Hasan, Y.-D. Chuang, A. Kuprin, Y. Kong, D. Qian, Y. W. Li, B. Mesler, Z. Hussain, A. V. Fedorov, R. Kimmerling, E. Rotenberg, K. Rossnagel, H. Koh, N. S. Rogado, M. L. Foo and R. J. Cava, *Phys. Rev. Lett.* **92** (2004) 246402.
- 44) H.-B. Yang, S.-C. Wang, A. K. P. Sekharan, H. Matsui, S. Souma, T. Sato, T. Takahashi, T. Takeuchi, J. C. Campuzano, R. Jin, B. C. Sales, D. Mandrus, Z. Wang and H. Ding, *Phys. Rev. Lett.* **92** (2004) 246403.
- 45) M. Karppinen, I. Asako, T. Motohashi and H. Yamauchi, cond-mat/0402484.
- 46) M. Sigrist and K. Ueda, *Rev. Mod. Phys.* **63** (1991) 239.
- 47) K. Kuroki, T. Kimura, R. Arita, Y. Tanaka and Y. Matsuda, *Phys. Rev. B* **65** (2002) 100516(R).
- 48) Y. Tanaka, Y. Yanase and M. Ogata, to appear in *J. Phys. Soc. Jpn.*
- 49) R. E. Schaak, T. Klimczuk, M. L. Foo and R. J. Cava, *Nature*, **424** (2003) 527.
- 50) C. J. Milne, D. N. Argyriou, A. Chemseddine, N. Aliouane, J. Veira and D. Alber, cond-mat/0401273.
- 51) M. D. Johannes, I. I. Mazin, D. J. Singh and D. A. Panacon-

stantopoulos, cond-mat/0403135.

52) H. Takahashi, J. Phys. Soc. Jpn. **68** (1999) 194; Y. Onishi and K. Miyake, J. Phys. Soc. Jpn. **68** (1999) 3927.

53) T. Nomura and K. Yamada: J. Phys. Soc. Jpn. **71** (2002) 404.

54) J. Kanamori, Prog. Theor. Phys. **30** (1963) 275.

55) N. Bulut, Adv. Phys. **51** (2002) 1587.

56) T. Nomura and K. Yamada, J. Phys. Soc. Jpn. **72** (2003) 2053.

57) K. Ishida, private communication.

58) G.-Q. Zheng and Y. Kitaoka, private communication.

59) T. Sasaki, P. Badica, N. Yoneyama, K. Yamada, K. Togano and N. Kobayashi, J. Phys. Soc. Jpn. **73** (2004) 1131.

60) K. Kuroki, private communication.

61) M. Yokoi, H. Watanabe, Y. Mori, T. Moyoshi, Y. Kobayashi and M. Sato, J. Phys. Soc. Jpn. **73** (2004) 1297.